The versatility of asymmetric aminoethyl-tetrazines in bioorthogonal chemistry

Sarris, A.

Chapter 5: Fast and pH-independent elimination of *trans*-cyclooctene using aminoethyl functionalized tetrazines

Introduction

Inverse electron demand Diels-Alder (IEDDA)-pyridazine elimination tandem reactions, in which the allylic substituent on *trans*-cyclooctene is eliminated following reaction with tetrazines, are gaining interest as a versatile bioorthogonal process. One potential shortcoming of the currently used reactions is their propensity to run faster and more efficient at increasing acidity of the reaction medium. This feature, caused by the nature of the tetrazines used in these contemporary studies, dictates that at biologically relevant pH (ranging broadly from 4 to 7) IEDDA-based elimination/biological activation processes may proceed at a suboptimal speed. In this chapter, aminoethyl substituted tetrazines are presented as the first pH-independent reagents showing invariably fast elimination kinetics at all biologically relevant pH's.

Bioorthogonal chemistry – the execution of selective chemical conversions within a biological sample – has provided a wealth of information on a wide variety of biological processes.[1] Initial work included the controlled ligation reactions within biological systems. Examples of such bioorthogonal ligations include copper-catalyzed Huisgen cycloadditions[2], Staudinger ligations[3], inverse electron demand Diels-Alder (IEDDA) reactions[4], amongst other chemistries[5]. Bioorthogonal ligations have found wide application in adding a reporter group after a biochemical/biological process or pathway has run to completion. In this instance, one of the bioorthogonal reaction partners, ideally a modified substrate containing a metbolically inert and small moiety (alkyne, azide, cyclopropene, respective towards the above mentioned bioorthogonal ligation reactions), is engineered within the molecule of interest that is processed by the biological system of interest. Such entity, when compared to the final reporter moiety (a fluorophore, biotin or any other type of tag), has a much better chance to proceed through the physiological process or pathway similar to the unmodified substrate. The ligation itself should proceed with high speed and efficiency (also in terms of side reactions which should be minimal) to maximize sensitivity in detection and minimize false positives (for instance due to side reactions).

Bioorthogonal reactions have also been used to unmask functional groups in living systems.[6] A molecule of interest is rendered biologically inert by introducing a chemical functionality masking the natural functional group. The molecule can then be re-activated by removing the introduced masking chemical group using the bio-oorthogonal reaction partner. In bioorthogonal ligation, and perhaps even more so in bioorthogonal elimination, reaction speed and selectivity are essential.

The IEDDA-pyridazine elimination reaction[7] – a "click-to-release" reaction by which an allylic substituent on *trans*-cyclooctene (2-TCO, axial (E)-cyclooct-2-en-1-ol) is eliminated upon rearrangement of the pyridazine intermediate – has proven particularly favorable in this regard. Depening on the nature of the chosen IEDDA reaction pair (diene, and dienophile), it has excellent biocompatibility[9] and low toxicity[10]. *In vivo* applications include chemical control of drug release[11], control over T-cell activation[8], release of drugs from hydrogels[12], as well as the control over kinase activity in mice[10]. The use of this reaction for the localised release of a chemotherapeutic is now even pursued in human clinical trials.[15]

Mechanistic insight into the IEDDA click-to-release reaction has provided a pathway towards its improvement (**Figure 1**).[13] Chen and co-workers, for example, discovered that asymmetric tetrazines carrying both an electron-donating and electron-withdrawing substituent showed a significant improvement in the elimination rates compared to their symmetric counterparts, leading to improved results of their most prominent tetrazine **1** over 3,6-dimethyl tetrazine **2**[13a]. Weissleder and co-workers used carboxy-functionalized tetrazine **3** and observed elimination rates much faster than tetrazine **2**.[13b] It was also discovered that, for tetrazines containing simple alkyl substituents, elimination rates are very sensitive to the pH of the reaction medium: while release is completed within an hour at acidic conditions (tetrazine **2**, pH 5.0), it takes several hours under physiological conditions (tetrazine **2**, pH 7.0)[13b], as the elimination step is subject to general acid catalysis. What was lacking at the onset of these studies were tetrazines that maintain fast elimination kinetics over the whole biologically relevant pH range (pH 3.5 – pH 7.5). It was postulated that tetrazines **4**, **5**, **6**, **7** and **17** could serve as pH-independent eliminating tetrazines. The amine on the aminoethyl substituent, as cationic ammonium functionality at and below physiological pH, would function as general acid during the elimination step, potentially improving both release rate and efficiency.

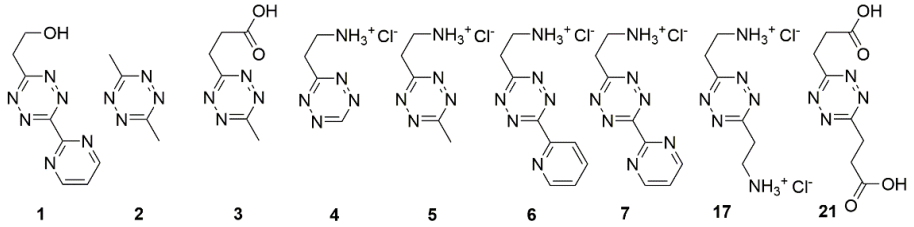

Figure 1. Known tetrazines (**1**, **2**, **3** and **21**) and aminoethyl substituted tetrazines (**4**, **5**, **6**, **7** and **17**) synthesized in chapter 3.

In this chapter the elimination behavior of the family of aminoethyl tetrazines synthesized in **chapter 3** are explored. It is shown that, through intramolecular proton delivery, an increase in the elimination rate by 18-fold compared to the fastest reported literature tetrazines **1** and **3** could be attained. Furthermore, this intramolecular proton source renders the reaction pH independent with minimal change in the reaction rates from pH 3 to pH 7.4.

Design

Based on the functional groups present on the synthesized tetrazines from chapter 3, a selection was made focusing on aminoethyl functioalized tetrazines. Similar to tetrazines having a carboxylate functionality,[13b] an aminoethyl could possibly catalyze both the 4,5- to 1,4-tautomerization and subsequent elimination process (**Scheme 1**). The [4+2] IEDDA cycloaddition of an assymetric tetrazine (with respect to the substitutents at C2 and C5) with a 2-TCO can proceed with the aminoethyl functionality ending up at either the eliminating end (**A**, "head-to-head"), or the non-eliminating end (**B**, "head-to-tail") of the adduct. In the "head-to-head" adduct a tautomerisation of the initial 4,5-tautomer may be promoted leading to either the eliminating (**C**) 1,4-tautomer or the non-eliminating (**D**) 2,5-tautomer. Elimination (**E**) may then be driven through the proximity of the intramolecular catalytic amine (acting as a base) near both the N-1 of the dihydropyridazine core and carbamate linkage.

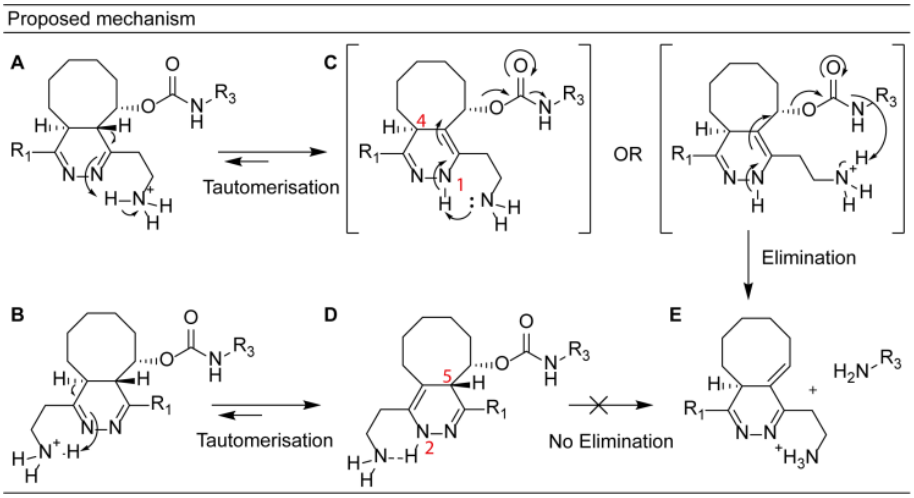

Scheme 1. Proposed mechanism for the tautomerisation and subsequent elimination via intramolecular catalysis by aminoethyl functionality.

To investigate the behavior of tetrazines **4**-**7** during addition and subsequequent elimination density functional theory (DFT) calculations were performed on the

transition states of these tetrazines (**Figure 1** and **2**)[14]. The transition states of the cycloaddition step for tetrazines **2** and **4-7** was evaluated computationally in reaction with a model alpha-carbamate modified *trans*-cylooctene (**Figure 1a-b**). The results suggest that the IEDDA reaction path towards the "head-to-head" adduct is favoured over the reaction path that leads to the "head-to-tail" adduct for all calculated aminoethyl functionalized tetrazines. In the "head-to-head" transition states the cationic ammonium functionality indeed interacts with the carbamate linkage resulting in an energetically favorable approach. For example, the "head-to-head" transition state (TS-1, **Figure 1a**) for tetrazine **5** proved to be 2.5 kcal/mol lower than the "head-to-tail" transition state (TS-2, **Figure 1a**). The thermodynamic preferences for the other aminoethyl tetrazines **4**, **6**, **7** appeared to be even greater at 4.4 - 4.6 kcal/mol (**Figure 1a-b**).

After establishing the theoretically favored geometries of the transition state in the cycloaddition step, the lowest energy geometries of the formed adducts were investigated (**Figure 2**). From these calculations it follows that tautomerization from initial 4-5-dihydropyridazine towards eliminating 1,4-dihydropyridazine appears energetically favorable and shows prominent interaction between the aminoethyl functionality and the N-1 of the dihydropyridazine core in both neutral (**Figure 2A**) and cationic (**Figure 2B**) state. The hypothetical proton transfer through a six-membered-cyclic-transition-state is geometrically feasible in the kinetically favored "head-to-head" adduct and likely to facilitate both tautomerization and elimination (**Scheme 1**). The design consideration described above, supported by the calculations, indicated that the tetrazines **4-7** would show fast and pH independent kinetics for the "click-to-release" reaction.

Tetrazine 2

TS

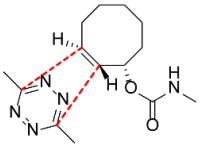

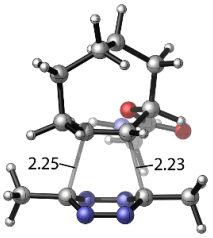

$\Delta G^{\ddagger}_{aq}$ (kcal/mol)	20.6
ν_i (cm^{-1})	-408.0i

Tetrazine 4

TS1 - "Head-to-Head"

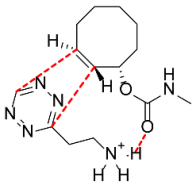

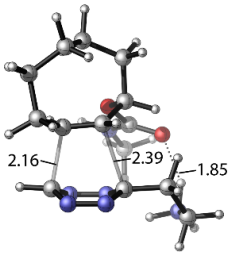

TS2 - "Head-to-Tail"

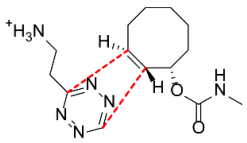

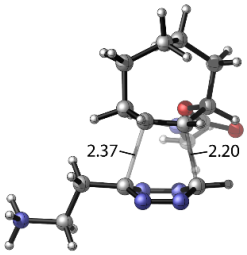

14.5	$\Delta G^{\ddagger}_{aq}$ (kcal/mol)	18.9
-368.8i	ν_i (cm^{-1})	-337.3i

Tetrazine 5

TS1 - "Head-to-Head"

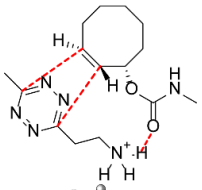

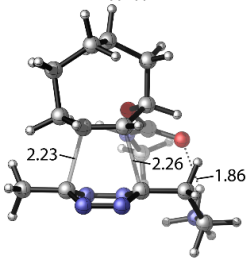

TS2 - "Head-to-Tail"

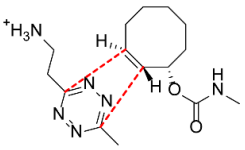

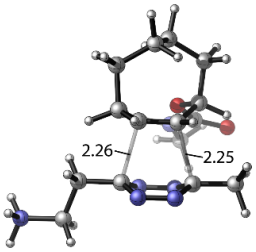

17.8	$\Delta G^{\ddagger}_{aq}$ (kcal/mol)	21.3
-403.5i	ν_i (cm^{-1})	-387.8i

Figure 1a: Transition states for "head-to-head" (**TS1**) and "head-to-tail" (**TS2**) reactions of tetrazines **2, 4** and **5** with model axial (E)-cyclooct-2-ene. Distances of interest (forming C-C bonds, interactions) are labelled in Å. Reported transition states were used for initial approximations.[14] All structures were optimized with Gaussian 09 using the ωB97XD long-range corrected hybrid functional and 6-31+G(d) as basis set. Optimization was done in combination with a polarizable continuum model (PCM) using water as solvent parameter.

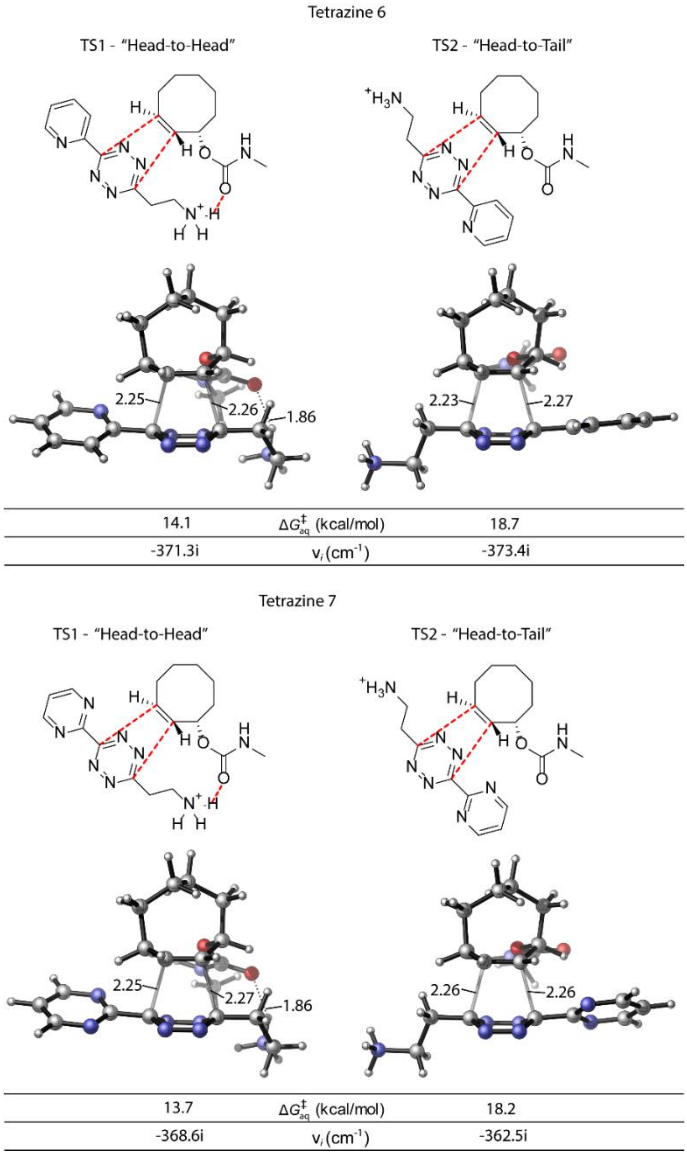

Figure 1b: Transition states for "head-to-head" (**TS1**) and "head-to-tail" (**TS2**) reactions of tetrazines **6** and **7** with model axial (E)-cyclooct-2-ene. Distances of interest (forming C-C bonds, interactions) are labelled in Å. Reported transition states were used for initial approximations.[14] All structures were optimized with Gaussian 09 using the ωB97XD long-range corrected hybrid functional and 6-31+G(d) as basis set. Optimization was done in combination with a polarizable continuum model (PCM) using water as solvent parameter.

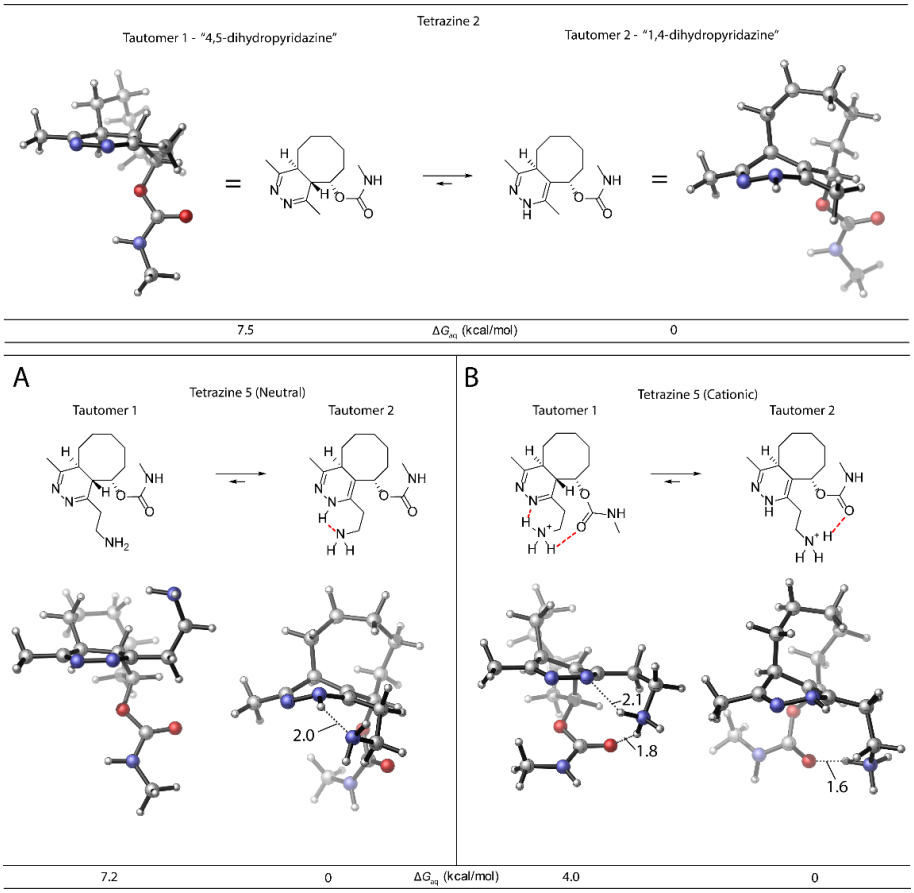

Figure 2. Lowest energy geometries of dihydropyridazine adducts. Proton transfer is geometrically feasible (red lines). **A**) "Neutral" Initial 4,5-tautomer (left) and thermodynamically favorable 1,4-tautomer (right) **B**) "Cationic" Initial 4,5-tautomer (left) and thermodynamically favorable 1,4-tautomer (right). Conformer distributions were generated with Spartan 10 program using molecular mechanics with MMFF94 as force field, for the formed initial 4,5-tautomer and subsequent 1,4-tautomer after cycloaddition of tetrazines **2** and **5** with model axial (E)-cyclooct-2-en. All generated structures were further optimized in the gas-phase with Gaussian 09 using the ωB97XD functional with 6-311G(d,p) basis set and optimized with PCM using water as solvent parameter.

Determination of elimination kinetics

To probe the importance of the intramolecular proton delivery by the aminoethyl functionality the efficacy of tetrazines **4**-**7** and **17** (**Figure 3B**), in a IEDDA-click to release reaction with trans-cyclooctene **X**, was compared to the efficacy of tetrazines from literature, known to be either of the "non-releasing" (**23**, **24**) or "releasing" (**1**, **2**, **25**) type (**Figure 3A**). Comparative studies with N-Boc protected tetrazines **4b**-**16b** (**Figure 3B-C**) and tetrazines **8**-**16** (**Figure 3D**), in which the amino group is expected to be unable to provide intramolecular assistance for geometrical reasons, were conducted as well.

To assess the elimination properties of all tetrazines a direct fluorescence-based assay[13a] that allows monitoring the reaction in real time was chosen (**Figure 4A**). This method was preferred over LC-MS based analysis[13a][13b] as it allows a rapid measurement of several tetrazines simultaneously, acquisition of more data (at the initial stage of the reaction) and is not affected by possible "pseudo-release" artefacts caused by LC-MS analysis.[13b] Tetrazine elimination properties were assessed through reaction with fluorogenic 2-TCO-modified 7-amino-4-methylcoumarin **28** (2-TCO-AMC)[13a] and tracking the product AMC **27** by measuring its characteristic fluorescence at 450 nm (**Figure 4B**).

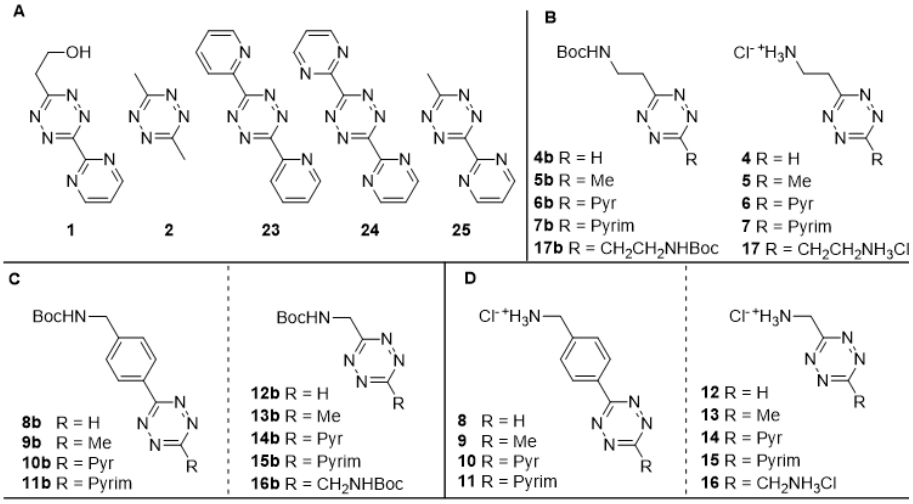

Figure 3. A) Tetrazines **1**, **2**, **23**-**25** used as literature references. B) Aminoethyl tetrazines **4**-**7** and **17**, and N-Boc protected aminoethyl tetrazines **4b**-**7b** and **17b**. C) N-Boc protected tetrazines **8b**-**16b**. D) tetrazines **8**-**16**.

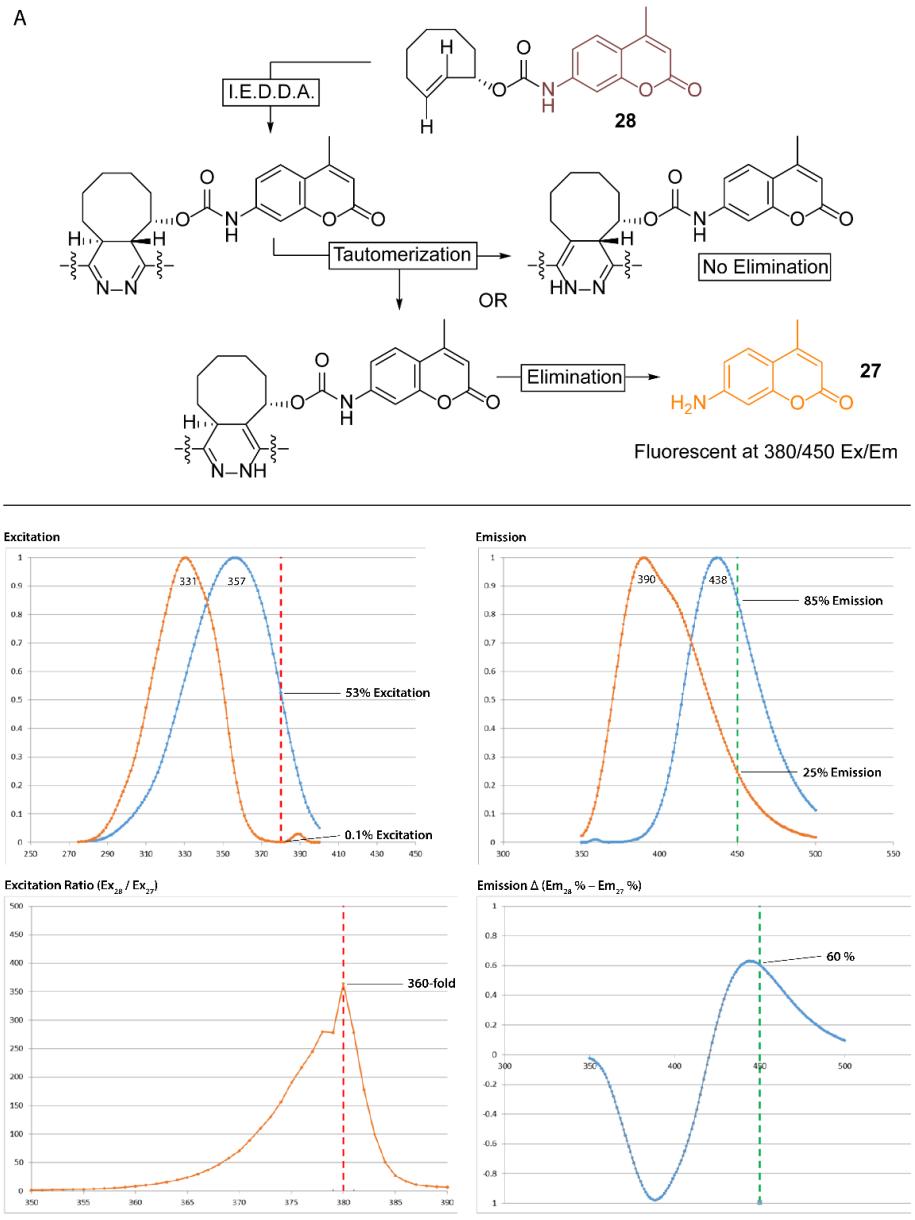

Figure 4 A) Fluorogenic assay: 2-TCO-AMC **28** is used as a measurement tool to track the release of fluorescent AMC **27** upon reaction with tetrazines. B) Normalized excitation (left) and emission (right) spectra of AMC **27** (blue) and 2-TCO-AMC **28** (orange). Chosen excitation wavelength (380nm, excitation ratio (Ex_{27} / Ex_{28}) = 360-fold) is visualized by the vertical red line. Chosen emission wavelength (450nm, Emission Δ (Em_{27} % – Em_{28} %) = 60%) is visualized by the vertical green line.

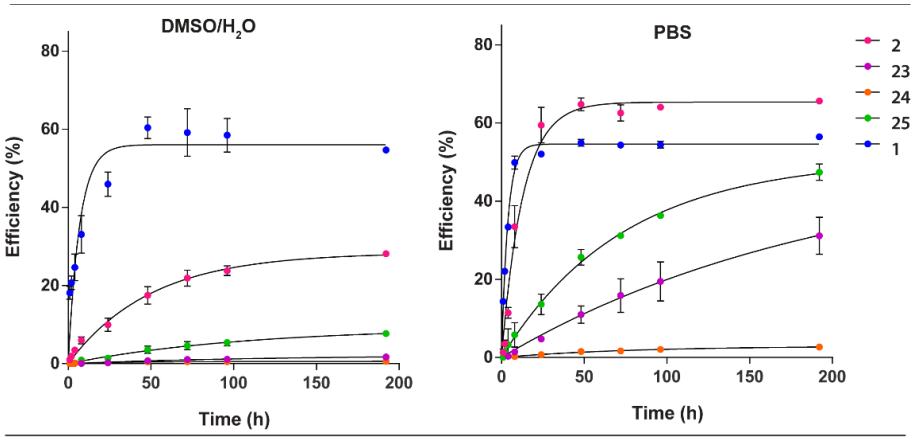

	DMSO/H_2O		PBS	
2	k_{elim} = 0.79 * 10^{-5} s^{-1}	Eff % = 28 %	k_{elim} = 2.91 * 10^{-5} s^{-1}	Eff % = 65 %
23	k_{elim} = 0.36 * 10^{-5} s^{-1}	Eff % = 2 %	k_{elim} = 0.15 * 10^{-5} s^{-1}	Eff % = 51 %
24	k_{elim} = 1.01 * 10^{-5} s^{-1}	Eff % = 1 %	k_{elim} = 0.62 * 10^{-5} s^{-1}	Eff % = 3 %
25	k_{elim} = 0.41 * 10^{-5} s^{-1}	Eff % = 9 %	k_{elim} = 0.47 * 10^{-5} s^{-1}	Eff % = 51 %
1	k_{elim} = 2.07 * 10^{-5} s^{-1}	Eff % = 56 %	k_{elim} = 8.86 * 10^{-5} s^{-1}	Eff % = 55 %

Figure 5: Corrected normalized elimination efficiency over time of tetrazines **1, 2, 23, 24** and **25** in DMSO/H_2O (1:1, v:v) and PBS (0.25% DMSO). Maximum elimination efficiencies (Eff %) were determined by first-order exponential decay approximations (black lines).

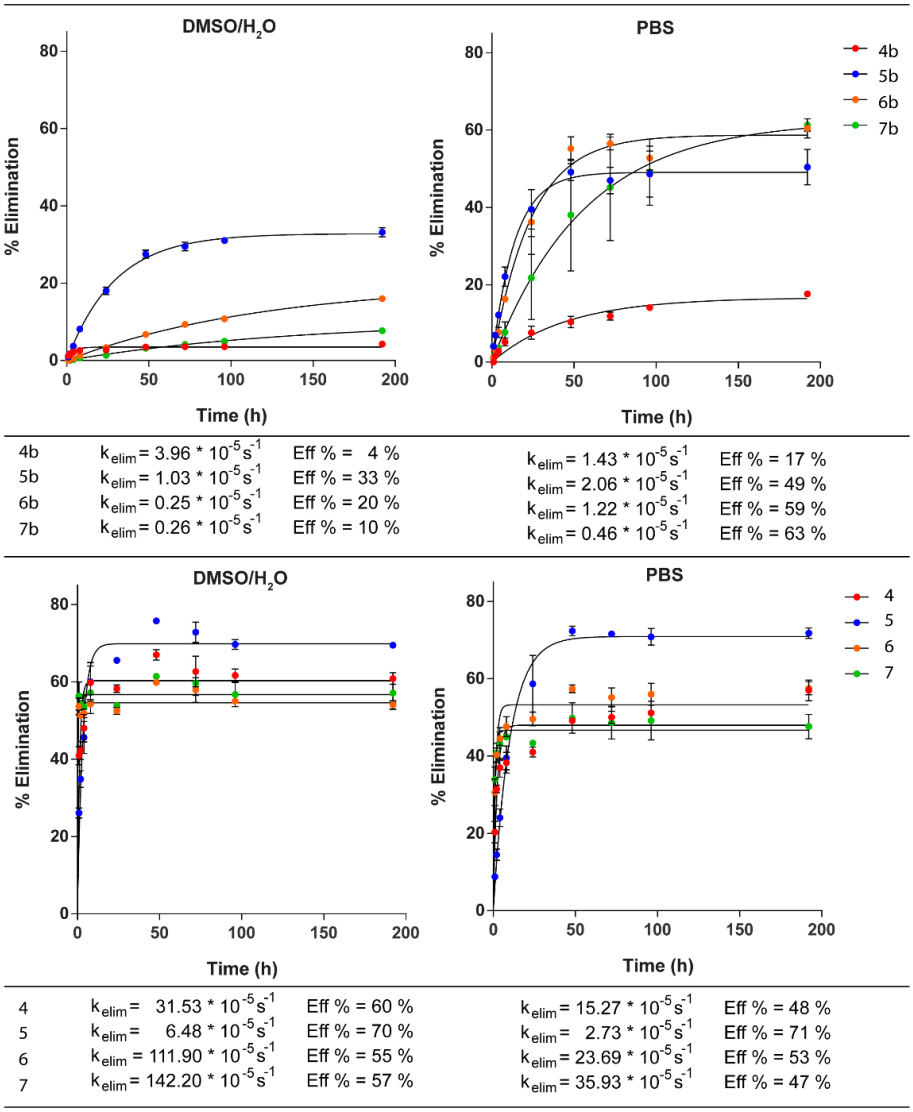

	DMSO/H_2O		PBS	
4b	k_{elim} = 3.96 * 10^{-5} s^{-1}	Eff % = 4 %	k_{elim} = 1.43 * 10^{-5} s^{-1}	Eff % = 17 %
5b	k_{elim} = 1.03 * 10^{-5} s^{-1}	Eff % = 33 %	k_{elim} = 2.06 * 10^{-5} s^{-1}	Eff % = 49 %
6b	k_{elim} = 0.25 * 10^{-5} s^{-1}	Eff % = 20 %	k_{elim} = 1.22 * 10^{-5} s^{-1}	Eff % = 59 %
7b	k_{elim} = 0.26 * 10^{-5} s^{-1}	Eff % = 10 %	k_{elim} = 0.46 * 10^{-5} s^{-1}	Eff % = 63 %
4	k_{elim} = 31.53 * 10^{-5} s^{-1}	Eff % = 60 %	k_{elim} = 15.27 * 10^{-5} s^{-1}	Eff % = 48 %
5	k_{elim} = 6.48 * 10^{-5} s^{-1}	Eff % = 70 %	k_{elim} = 2.73 * 10^{-5} s^{-1}	Eff % = 71 %
6	k_{elim} = 111.90 * 10^{-5} s^{-1}	Eff % = 55 %	k_{elim} = 23.69 * 10^{-5} s^{-1}	Eff % = 53 %
7	k_{elim} = 142.20 * 10^{-5} s^{-1}	Eff % = 57 %	k_{elim} = 35.93 * 10^{-5} s^{-1}	Eff % = 47 %

Figure 6a: Corrected normalized elimination efficiency over time of tetrazines **4b**-**7b** and **4**-**7** in DMSO/H_2O (1:1, v:v) and PBS (0.25% DMSO). Maximum elimination efficiencies (Eff %) were determined by first-order exponential decay approximations (black lines).

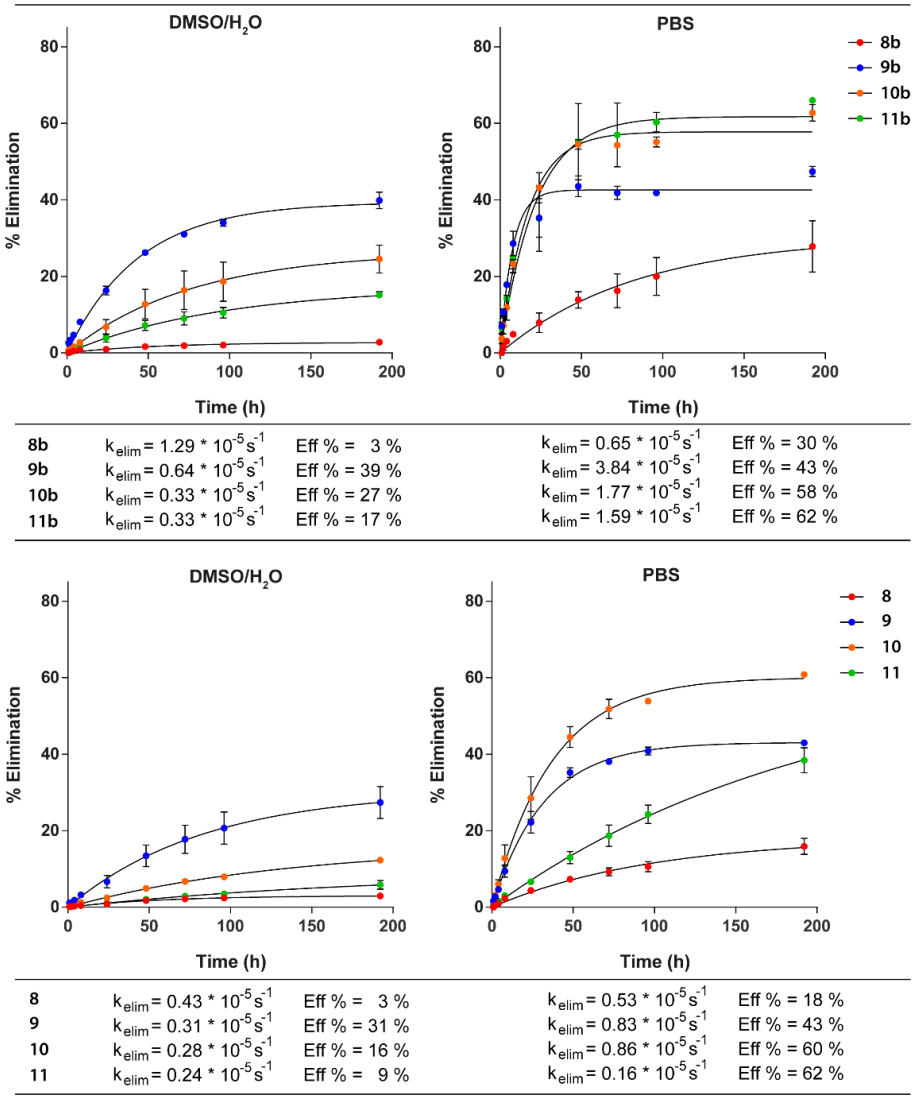

	DMSO/H_2O		PBS	
8b	k_{elim} = 1.29 * 10^{-5} s^{-1}	Eff % = 3 %	k_{elim} = 0.65 * 10^{-5} s^{-1}	Eff % = 30 %
9b	k_{elim} = 0.64 * 10^{-5} s^{-1}	Eff % = 39 %	k_{elim} = 3.84 * 10^{-5} s^{-1}	Eff % = 43 %
10b	k_{elim} = 0.33 * 10^{-5} s^{-1}	Eff % = 27 %	k_{elim} = 1.77 * 10^{-5} s^{-1}	Eff % = 58 %
11b	k_{elim} = 0.33 * 10^{-5} s^{-1}	Eff % = 17 %	k_{elim} = 1.59 * 10^{-5} s^{-1}	Eff % = 62 %
8	k_{elim} = 0.43 * 10^{-5} s^{-1}	Eff % = 3 %	k_{elim} = 0.53 * 10^{-5} s^{-1}	Eff % = 18 %
9	k_{elim} = 0.31 * 10^{-5} s^{-1}	Eff % = 31 %	k_{elim} = 0.83 * 10^{-5} s^{-1}	Eff % = 43 %
10	k_{elim} = 0.28 * 10^{-5} s^{-1}	Eff % = 16 %	k_{elim} = 0.86 * 10^{-5} s^{-1}	Eff % = 60 %
11	k_{elim} = 0.24 * 10^{-5} s^{-1}	Eff % = 9 %	k_{elim} = 0.16 * 10^{-5} s^{-1}	Eff % = 62 %

Figure 6b: Corrected normalized elimination efficiency over time of tetrazines **9b**-**11b** and **9**-**11** in DMSO/H_2O (1:1, v:v) and PBS (0.25% DMSO). Maximum elimination efficiencies (Eff %) were determined by first-order exponential decay approximations (black lines).

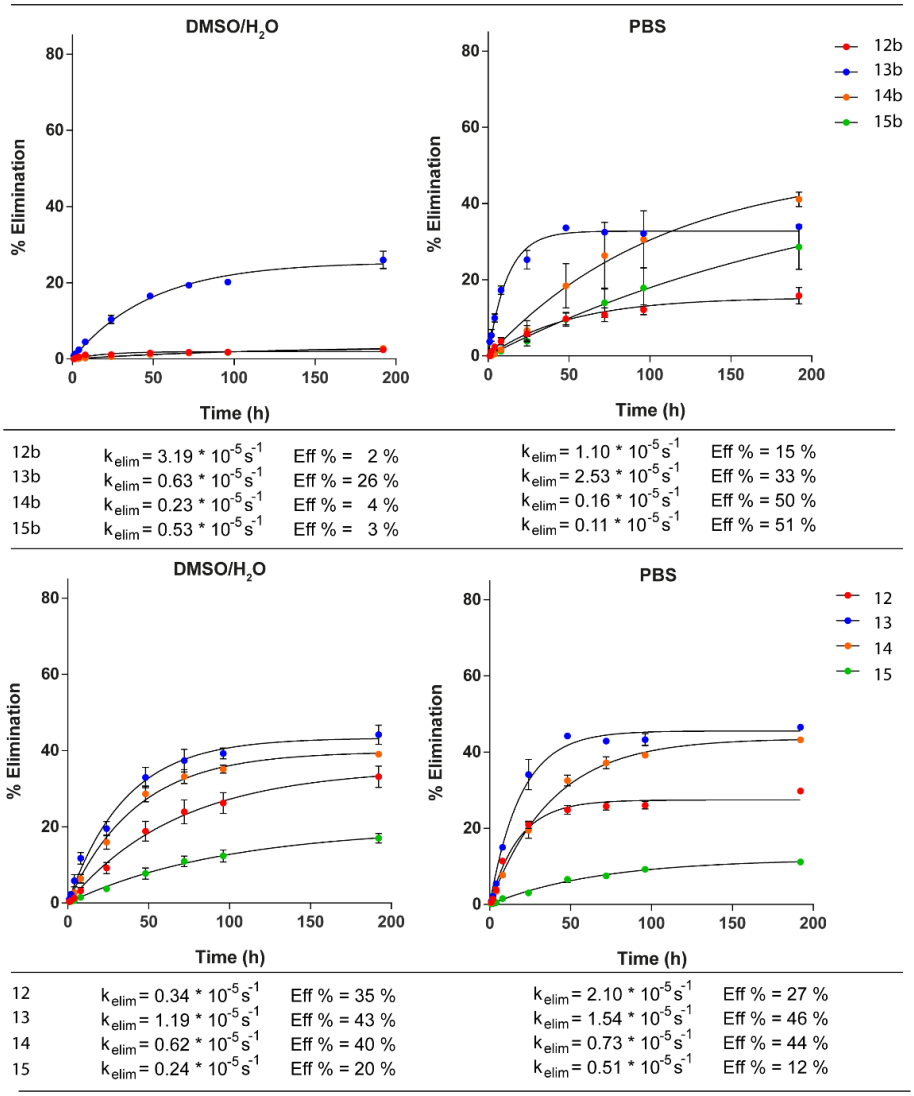

	DMSO/H_2O		PBS	
12b	k_{elim} = 3.19 * 10^{-5} s^{-1}	Eff % = 2 %	k_{elim} = 1.10 * 10^{-5} s^{-1}	Eff % = 15 %
13b	k_{elim} = 0.63 * 10^{-5} s^{-1}	Eff % = 26 %	k_{elim} = 2.53 * 10^{-5} s^{-1}	Eff % = 33 %
14b	k_{elim} = 0.23 * 10^{-5} s^{-1}	Eff % = 4 %	k_{elim} = 0.16 * 10^{-5} s^{-1}	Eff % = 50 %
15b	k_{elim} = 0.53 * 10^{-5} s^{-1}	Eff % = 3 %	k_{elim} = 0.11 * 10^{-5} s^{-1}	Eff % = 51 %
12	k_{elim} = 0.34 * 10^{-5} s^{-1}	Eff % = 35 %	k_{elim} = 2.10 * 10^{-5} s^{-1}	Eff % = 27 %
13	k_{elim} = 1.19 * 10^{-5} s^{-1}	Eff % = 43 %	k_{elim} = 1.54 * 10^{-5} s^{-1}	Eff % = 46 %
14	k_{elim} = 0.62 * 10^{-5} s^{-1}	Eff % = 40 %	k_{elim} = 0.73 * 10^{-5} s^{-1}	Eff % = 44 %
15	k_{elim} = 0.24 * 10^{-5} s^{-1}	Eff % = 20 %	k_{elim} = 0.51 * 10^{-5} s^{-1}	Eff % = 12 %

Figure 6c: Corrected normalized elimination efficiency over time of tetrazines **12b**-**15b** and **12**-**15** in DMSO/H_2O (1:1, v:v) and PBS (0.25% DMSO). Maximum elimination efficiencies (Eff %) were determined by first-order exponential decay approximations (black lines).

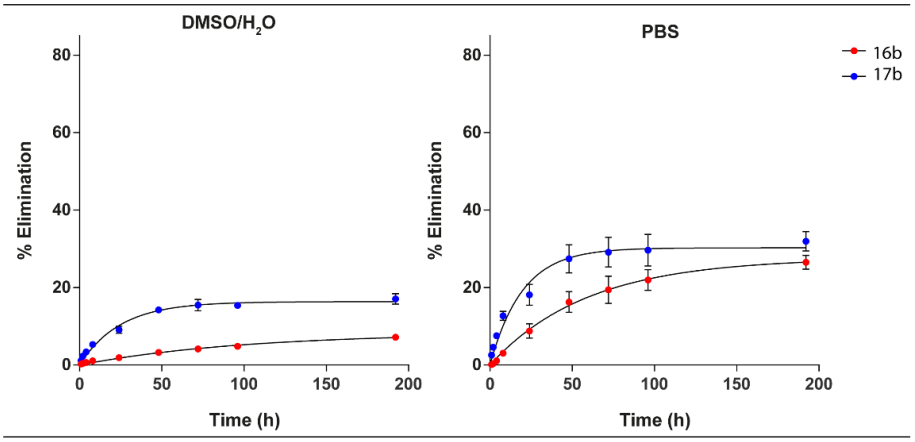

16b	k_{elim} = 0.42 * 10^{-5} s^{-1}	Eff % = 8 %	k_{elim} = 0.45 * 10^{-5} s^{-1}	Eff % = 28 %
17b	k_{elim} = 1.23 * 10^{-5} s^{-1}	Eff % = 16 %	k_{elim} = 1.80 * 10^{-5} s^{-1}	Eff % = 30 %

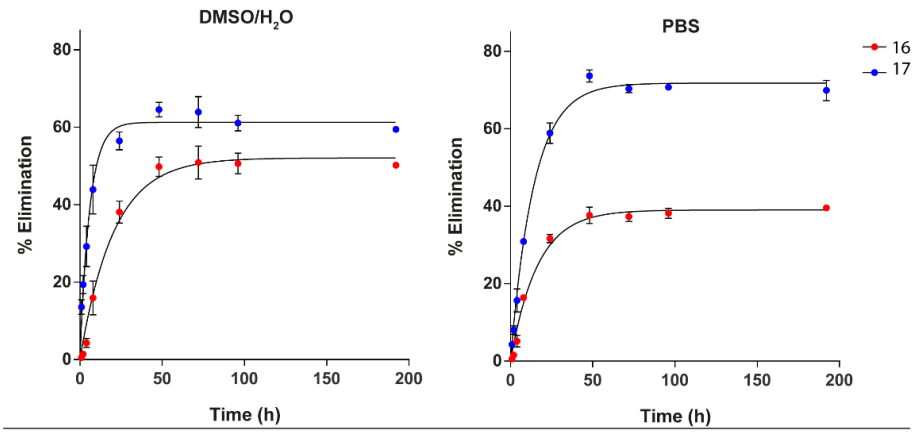

16	k_{elim} = 1.48 * 10^{-5} s^{-1}	Eff % = 52 %	k_{elim} = 3.16 * 10^{-5} s^{-1}	Eff % = 39 %
17	k_{elim} = 4.31 * 10^{-5} s^{-1}	Eff % = 61 %	k_{elim} = 2.01 * 10^{-5} s^{-1}	Eff % = 72 %

Figure 6d: Corrected normalized elimination efficiency over time of tetrazines **16b**-**17b** and **16**-**17** in DMSO/H_2O (1:1, v:v) and PBS (0.25% DMSO). Maximum elimination efficiencies (Eff %) were determined by first-order exponential decay approximations (black lines).

The elimination efficiency (Eff %) and rate (k_{elim}) of the tetrazine library was determined by exposing 2-TCO-AMC **28** (5 µM) to 4 equivalents (20 µM) of a tetrazine in PBS (pH 7.4) at 37 °C for 8 days (**Figures 6**, **7**). The solvent and concentrations were chosen to be either comparable to previous literature (DMSO/H2O) or relevant to experiments conducted in biological systems (PBS). Initially we tested the literature tetrazines **1**, **2**, **23**, **24** and **25** in both DMSO/H_2O (1:1, v:v) and PBS (0.25% DMSO) (**Figure 5**, top panels), followed by tetrazines **4b-7b**, **4-7** (Figure 6a), tetrazines **8b-11b**, **8-11** (**Figure 6b**), tetrazines **12b-15b**, **12-15** (**Figure 6c**) and tetrazines **16b-17b**, **16-17** (**Figure 6d**) under the same conditions. At various time points, the fluorescence intensity relative to 2-TCO-AMC **28** (0%) and AMC **27** (100%) was quantified from which the efficiency could be determined (Figures 5, 6, Eff% values). The results were then normalized and compared to each other. Linear approximations (black lines) were analysed, from which the elimination rate constants were extracted. Elimination rate constants (**Figure 5**, **6**, k_{elim} values) were determined for each tetrazine following first order rate equations:

$$\ln([\text{Tetrazine}]_t) = -k_{elim} * t - \ln([\text{Tetrazine}]_{t=0})$$

The obtained elimination properties of the tetrazine library in PBS were vastly different compared to DMSO/H_2O. Tetrazine **2**, for example, was both faster and more efficient in PBS. As a result, the further focus was on the experiments conducted in PBS.

The values for all tetrazines were plotted as dots in an XY-scatterplot as k_{elim} (logarithmic scale) vs Eff% (linear scale) (**Figure 7**, XY-scatterplot). Three classes of tetrazines were most conspicuous: **14b**, **15b**, **23**, **11** caused slow elimination rates ($k_{elim} < 0.20 * 10^{-5}$ s^{-1}; **Figure 7B**). **11b**, **2**, **5**, **17** all displayed intermediate elimination rates (k_{elim} between 1.5 and 3.0 * 10^{-5} s^{-1}; **Figure 7C**). Tetrazines **1**, **4**, **6**, **7** formed a third, most interesting, class of tetrazines defined by their very fast release kinetics (**Figure 7D**). While reference tetrazine **1** is fast (k_{elim} = 8.86 * 10^{-5} s^{-1}), it is still significantly slower compared to **4**, **6**, and **7** (k_{elim} = 15.3, 23.7, 35.9 10^{-5} s^{-1} respectively). Release rates for tetrazines **4**, **6** and **7** were too fast to be accurately determined by the initial assay and have therefore been displayed as the rate they are at minimum. It is noteworthy that the tetrazines with the protected amino group (**14b**, **15b**) and the tetrazines with a suboptimal positioned amino group (**11**) showed slow elimination rates (**Figure 7B**). This behavior proved to be general across the whole test set (**Figures 5**, **6**) and underscores the importance of the intramolecular proton delivery for the rate of the “click-to-release” process.

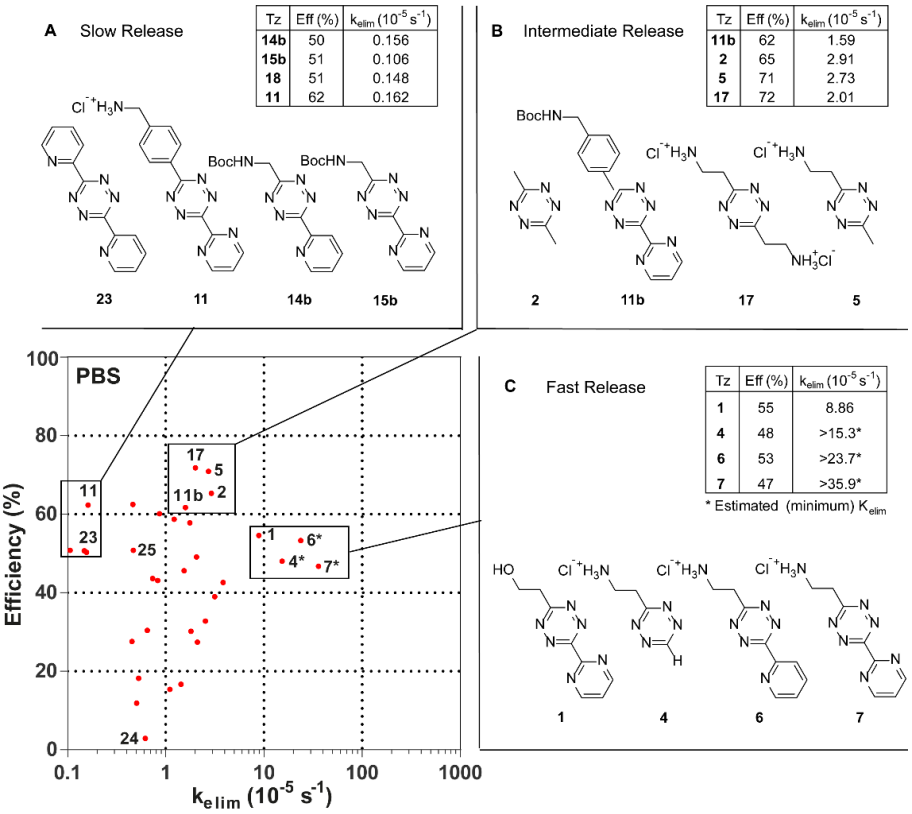

Figure 7: A) XY-scatterplot of all data obtained in PBS as solvent during the fluorescence-based assay. Each result (tetrazines **1**, **2**, **23**-**25**, **4b**-**17b**, **4**-**17**) is depicted as a dot based on their elimination efficiency and rate. B) Tetrazines **14b**, **15b**, **23** and **11** with slow release properties k_{elim} < 0.2 * 10^{-5} s^{-1}. C) Tetrazines **11b, 2**, **5** and **17** with intermediate release properties: Eff% > 60%. D) Tetrazines **1, 4**, **6** and **7** with fast release properties: k_{elim} > 8 * 10^{-5} s^{-1}.

pH dependency of elimination rates

Following these results we set out to determine whether the fast releasing aminoethyl functionalized tetrazines retained these properties over a wide pH-range. To this end, tetrazines **1**-**3**, **21**, **4b**-**7b** and **4**-**7** were exposed (**Figures 8**, **9**) to phosphate buffered solutions at various pH (0.2M [PO_4^{2-}], 10% DMSO, pH = 3.0 (red lines), 6.0 (green lines), and 7.4 (blue lines)) and the fluorescence intensity relative to 2-TCO-AMC **28** (0%) and AMC **27** (100%) was quantified at corresponding phosphate buffered solutions. At pH 3.0 (**Figure 10A**) all tetrazines showed elimination rates between 30 * 10^{-5} s^{-1} and 500 * 10^{-5} s^{-1}, indicating that the availability of protons in solution enhances the elimination rate. Lowering the proton concentration by raising pH to 6.0 or 7.4 resulted in large decreases in the elimination rates observed for most tetrazines (**Figure 10B**, **10C**). At pH 7.4 tetrazines **1**-**3**, **21**, **6b**, and **7b** showed much slower elimination rates (5-15 * 10^{-5} s^{-1}, **Figure 10C**, **10D**). Aminoethyl tetrazines **6** (k_{elim} = 241 * 10^{-5} s^{-1}) and **7** (k_{elim} = 120 * 10^{-5} s^{-1}) on the other hand showed a minimal reduction in rate at increased solvent pH (**Figure 10D**), resulting in a rate 18-27-fold faster at pH 7.4. Substituting amino (**6**, **7**) for alcohol (**1**) or carbamate (**6b, 7b**) functionality reintroduced pH-dependency in the elimination process (**Figure 11**). A carboxy functionality, as seen in tetrazine **3**, provided an overall moderate elimination rate and moderate pH-dependency (**Figure 11**).

Substitution of carboxy (**3**) for amino (**5**) functionality improved both properties. Furthermore, the fastest tetrazine **6** outperforms tetrazine **3** by 18-fold in terms of elimination rate. Finally, when comparing tetrazines **4-7**, the data also shows that the elimination rate is positively affected by electron-withdrawing substituents (pyridine/pyrimidine) explaining the differences between the tetrazines, in line with previous findings.[13b]

These results strongly support our hypothesis that the elimination process is dependent on proton availability and can be catalyzed at biologically relevant pH (3-7.4) through careful placement of cationic ammonium functionality acting as an intramolecular catalyst.

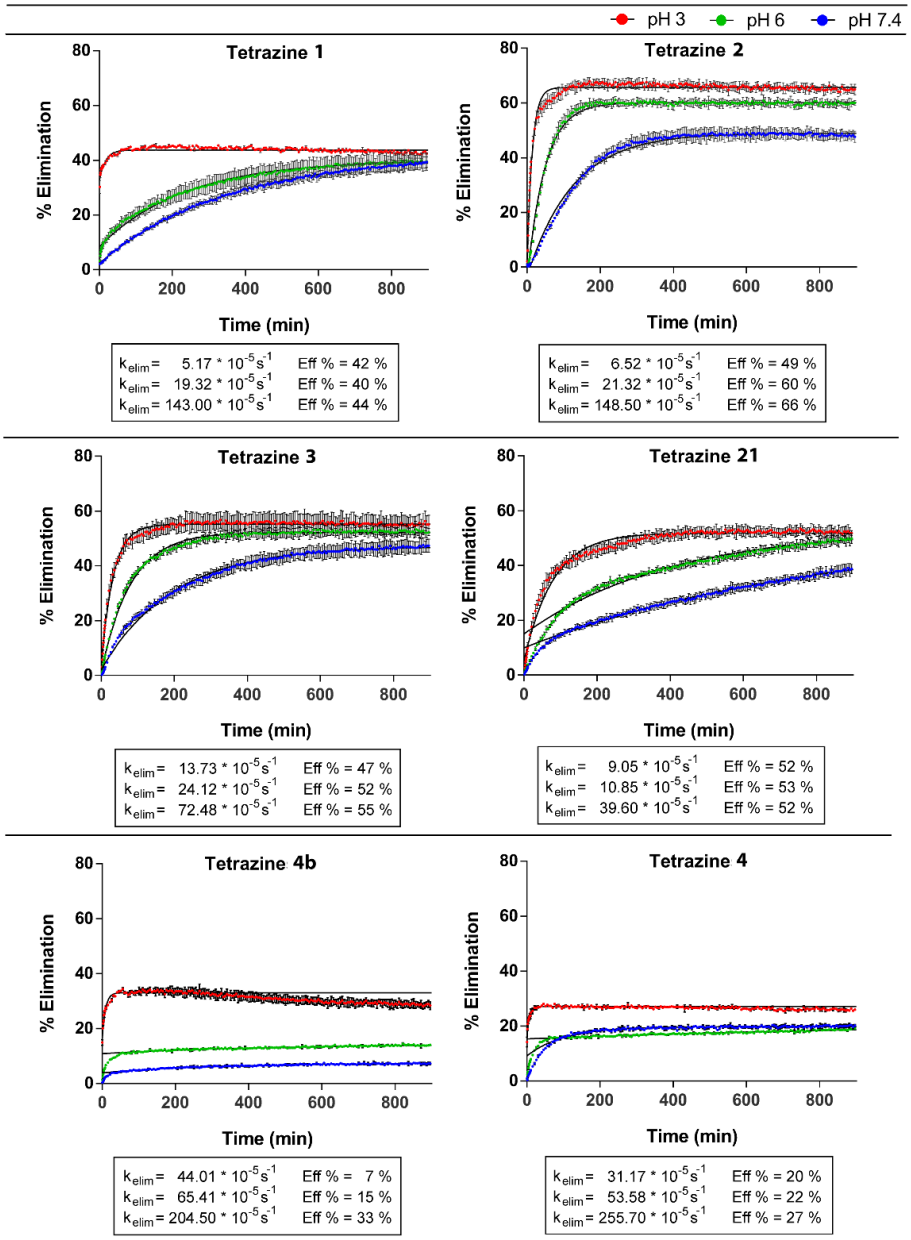

Figure 8: Corrected normalized elimination efficiency over time of tetrazines **1**, **2**, **3**, **21, 4b** and **4** in PBS at pH 3 (red), pH 6 (green) and pH 7.4 (blue). Maximum elimination efficiencies (Eff %) were determined by first-order exponential decay approximations (black lines).

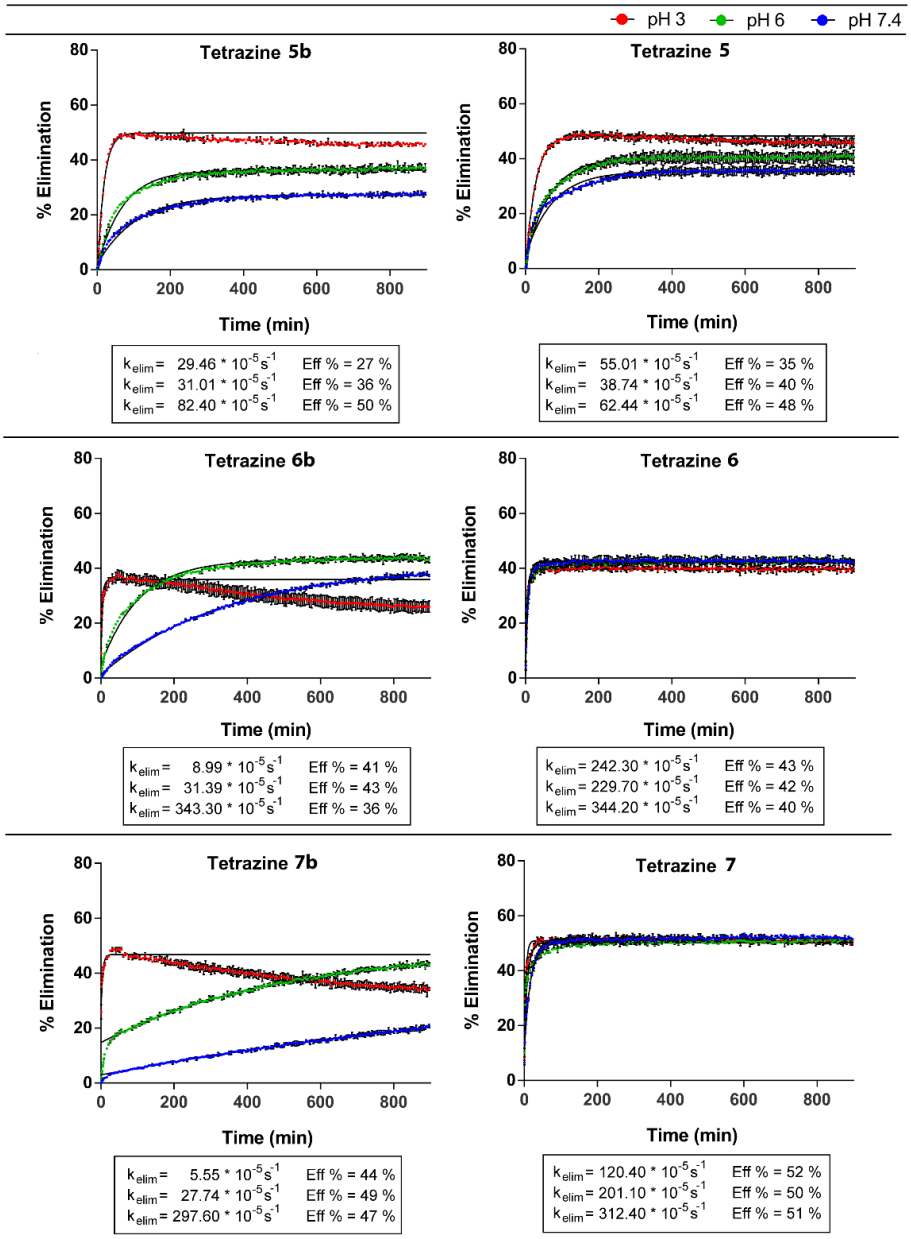

Figure 9: Corrected normalized elimination efficiency over time of tetrazines **5b**-**7b** and **5**-**7** in PBS at pH 3 (red), pH 6 (green) and pH 7.4 (blue). Maximum elimination efficiencies (Eff %) were determined by first-order exponential decay approximations (black lines).

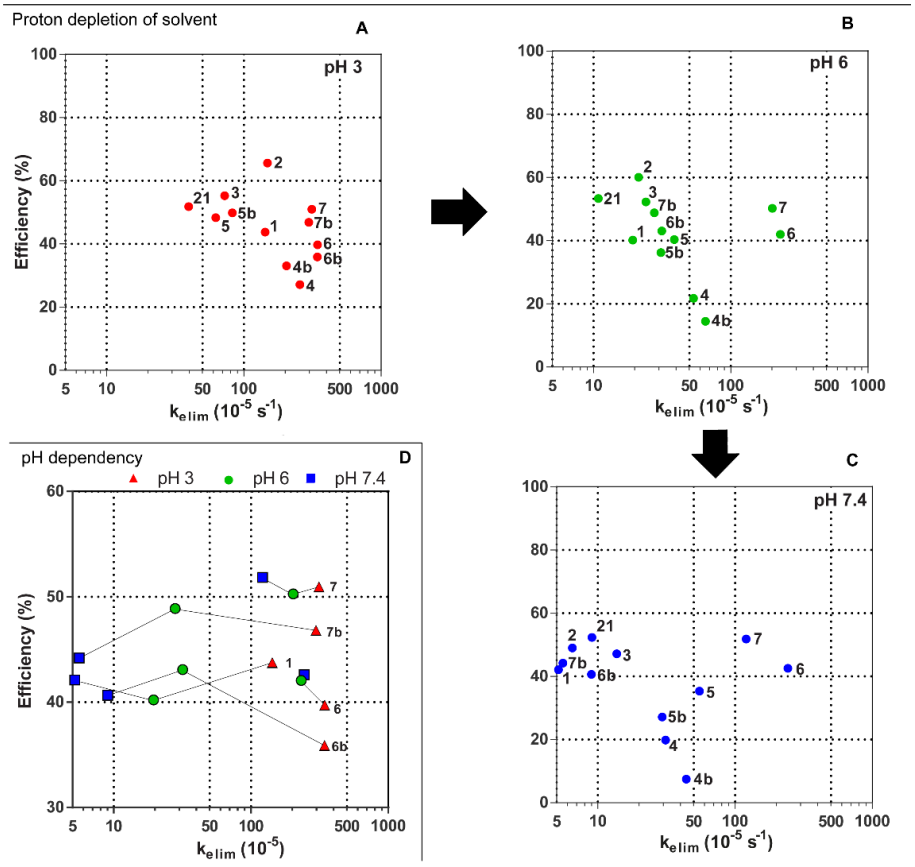

Figure 10. Proton depletion of solvent. A) Scatter plot of tetrazines at pH = 3. B) Scatter plot of tetrazines at pH = 6. C) Scatter plot of tetrazines at pH = 7.4. D) Scatter plot of pH dependent tetrazines (**6**, **7**) and pH independent tetrazines (**6b**, **7b**, **1**).

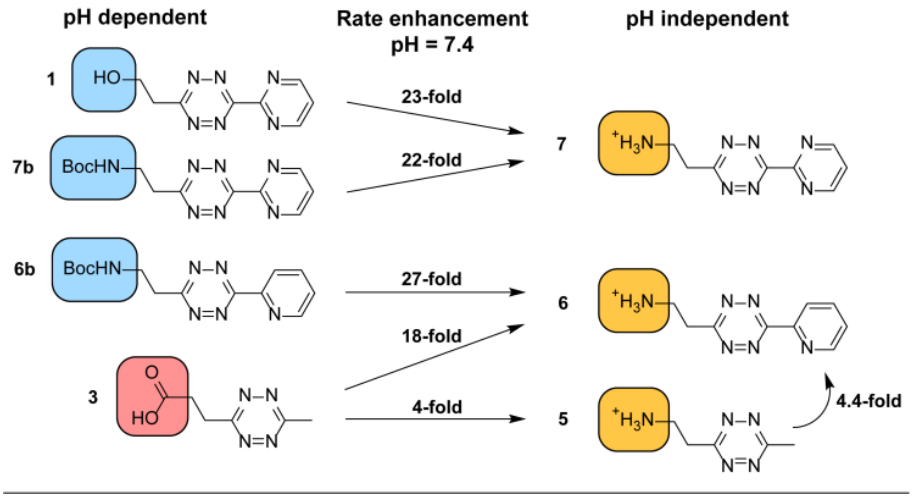

Figure 11. A) Rate enhancement of pH independent functional groups depicted in orange over pH dependent functional groups depicted in blue and red.

LC-MS analysis

In order to gain additional insight in the course of the "click-to-release" reaction with the newly developed aminoalkyl tetrazines and to study the intermediates and possible side products we also assessed the elimination rates of the key compounds **5 - 7** using reported LC-MS based approach that uses an ammonium formate buffered water-acetonitrile eluent (2.5mM $NH_4^+HCOO^-$, pH = 8.4) and taking the first analysis point at t = 5 min.[13b] Known tetrazines **1**-**3** were analyzed by this method for comparison. The elimination rates of tetrazines **2** and **3** showed results corresponding to data reported by Weissleder and coworkers[13b], where tetrazine **3** gives 48% release at t = 5 min, going up to 72% after 16 hours (Figure 12). The explanation offered by the authors invokes rapidly releasing "head-to-head" adduct and slowly releasing "head-to-tail" adduct which are formed in approximately equal amounts.[13b] The data showed much faster initial release than measured in the fluorescence assay, and this is likely due to additional "pseudo-release" or concentration effects during the LC-MS analysis. In turn, aminoethyl tetrazines **5**, **6** and **7**, showed 78%, 80% and 70% initial release respectively at t = 5 minutes with only a small further increase in release over time (Figure 12). This would correspond to the preferential formation of the rapidly releasing "head-to-head" adduct as predicted by our calculations.

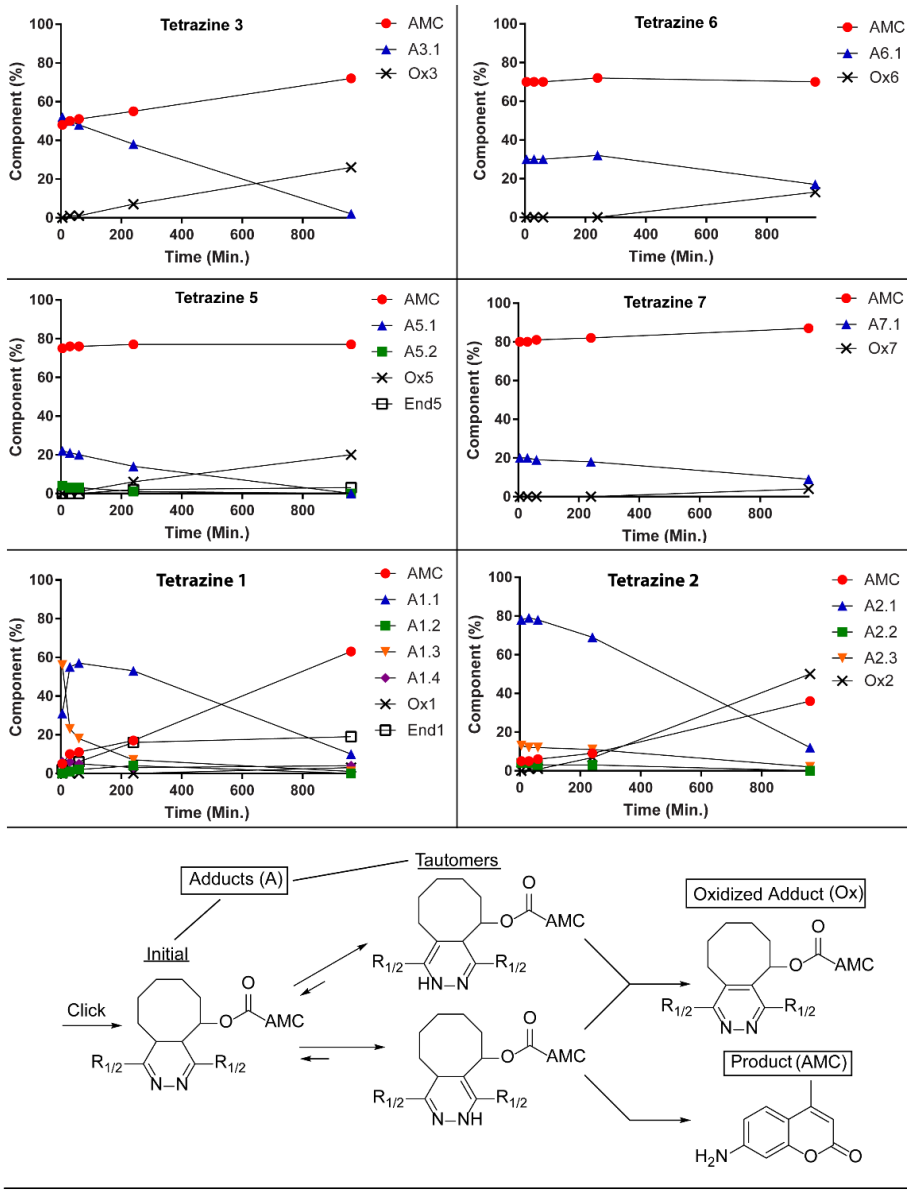

Figure 12. A) Time dependent LC-MS analysis of 2-TCO-AMC **28** with tetrazines **1**, **2**, **3**, **5**, **6** and **7** in PBS. **B)** Aminomethyl coumarin containing molecules: product "AMC", adduct "A", oxidized adduct "Ox" and dead-end adduct "End".

It is noteworthy that although multitude of different intermediates are observed, including putative “head-to-tail” and ”head-to-head” adducts, in the reaction of 2-TCO-AMC **28** with comparatively slow eliminating tetrazines **1** and **2** (Figure 12), as well as with tetrazines **3, 5, 6** and **7** (Figure 12), this does not translate into consistent formation of dead-end adduct (End) as reported by others[13b]. Furthermore the amount of oxidized adduct (Ox) is reduced for tetrazines **1**, **6**-**7** compared to tetrazines **2**, **3**, and **5**. The results of the LC-MS analysis of the “click-to-release” reaction of 2-TCO-AMC **28** with tetrazines **1** and **2** are similar to what is published by Robillard and co-workers in terms of observed intermediates and side products (Figure 12).[13c] To summarize this part, the results obtained from the LC-MS analysis of the key tetrazine derivatives demonstrate that the method shows reproducible results for the known tetrazines **2** and **3** and that the aminoethyl tetrazines **5**-**7** do perform as designed in the “click-to-release” IEDDA reaction.

Conclusions

The full kinetic profiling of a focused tetrazine library clearly shows that the presence of a properly placed cationic ammonium functionality acting as an intramolecular proton donor gives the tetrazine mediated “click-to-release” elimination a pH independent character. Asymmetric tetrazines that contain both this aminoethyl substituent and an electron-withdrawing substituent on the tetrazine core show unprecedented release rates combined with nearly complete pH independence over the whole biologically relevant pH range.

Computational Procedures

Geometry optimisation: IEDDA adduct structures

A conformer distribution search option included in the Spartan 10 program[17], with the use of MM with MMFF94 as force field, was used as starting point for the geometry optimization. All generated structures were further optimized with Gaussian 09[18] using the ωB97XD long-range corrected hybrid functional[19] and 6-311G(d,p) as basis set. Optimization was done in gas-phase and subsequently corrections for solvent effects were done by the use of a polarizable continuum model using water as solvent parameter. The electronic energies ΔE_{gas} were computed by dispersion-corrected DFT given by Equation (1), in which ΔE_{DFT} is the KS-DFT SCF energy and ΔE_{disp} is the standard atom pair-wise London dispersion energy.

$$\Delta E_{gas} = \Delta E_{DFT} + \Delta E_{disp} \quad (1)$$

The free Gibbs energy of the computed conformations was calculated using Equation (2) in which ΔE_{gas} is the gas-phase energy (electronic energy), ΔG^{T}_{RRHO} (T= 298.15 K and pressure= 1 atm.) is the sum of corrections from the electronic energy to free Gibbs energy in the rigid-rotor-harmonic-oscillator approximation (RRHO) also including zero-point-vibrational energy, and ΔG^{T}_{solv} is their corresponding free solvation Gibbs energy. Visualization of relevant structures was done with CYLview[20]. All denoted distances are expressed in ångström (Å).

$$\Delta G^{T}_{aq} = \Delta E_{gas} + \Delta G^{T}_{gas,RRHO} + \Delta G^{T}_{solv} \quad (2)$$

$$= \Delta G^{T}_{gas} + \Delta G^{T}_{solv}$$

Geometry optimization: IEDDA transition state structures

Initial guesses for the transition states were based on the work of Fox and co-workers and Houk and co-workers[21]. All generated structures were further optimized with Gaussian 09[18] using the ωB97XD long-range corrected hybrid functional[19] and 6-31+G(d) as basis set. Optimization was done in combination with a polarizable continuum model using water as solvent parameter.

General Synthetic Procedures

Preparation of anhydrous hydrazine 6.00 mol (300 mL) of hydrazine monohydrate was added to 3.6 mol (200 g) of KOH pellets, refluxed for 3 hours (>140 °C) and 5.5 mol (175 mL) hydrazine was collected via distillation (>140 °C). Then 175 mL of hydrazine was added to 75 mmol (30 g) NaOH pellets, refluxed for 1 hour (135 °C) and 3.7 mol (120 mL) of dry hydrazine was collected via distillation.

Procedure A (flask) First 1 eq. of R_1-CN nitrile reagent (**18**, **19** or **20**), 5 eq. of R_2-CN (formamidine acetate, acetonitrile, 2-cyano pyridine or 2-cyano pyrimidine) and 0.25 eq. of catalyst (zinc triflate, zinc iodide, or nickel triflate) were added to a flask under inert nitrogen atmosphere. Then (if used) dry dioxane (1.6 mL/mmol) was added. Anhydrous hydrazine (50 eq., 1.6 mL/mmol) was added dropwise under heavy stirring, while maintaining room temperature in a water bath. After 5 minutes (if required) the temperature was slowly

adjusted to the desired value. After the desired time a dihydrotetrazine containing reaction mixture was obtained.

Procedure B (pressure tube) First 1 eq. of R_1-CN nitrile reagent (**18**, **19** or **20**), 5 eq. of R_2-CN (formamidine acetate, acetonitrile, 2-cyano pyridine or 2-cyano pyrimidine) and 0.25 eq. of catalyst (zinc triflate, zinc iodide, or nickel triflate) were added to a pressure tube. Then (if used) dry dioxane (1.6 mL/mmol) was added. The tube was sealed and anhydrous hydrazine (50eq., 1.6 mL/mmol) was quickly injected under heavy stirring, while maintaining room temperature in a water bath. After 5 minutes (if required) the temperature was slowly adjusted to the desired value. After the desired time, the reaction was cooled to room temperature and the rubber seal was carefully punctured, slowly releasing the generated NH_3 gas. A dihydrotetrazine containing reaction mixture was obtained.

Procedure C (oxidation) A mixture of DCM/AcOH (1:1, v:v, 20 mL/mmol) was prepared. While stirring, the dihydrotetrazine containing reaction mixture was added dropwise. Solid $NaNO_2$ (20 eq., 1.5 g/mmol) was added portion wise over 30 minutes. The mixture was concentrated using rotary evaporation, re-dissolved in EtOAc, washed with H_2O ($NaHCO_3$ (aq.) or HCl (aq.)), dried using $MgSO_4$ and concentrated using rotary evaporation. The crude product was purified by column chromatography.

Procedure D (oxidation) The dihydrotetrazine containing reaction mixture was dissolved in 4M $NaNO_2$ (aq.) (40 eq., 10 mL/mmol) and 2M HCl (aq.) (60 eq., 30 mL/mmol) was added dropwise under heavy stirring until gas formation stops (pH = 2-3). Then 0.1M HCl (aq.) (50 mL/mmol) was added and the watery solution was extracted multiple times with EtOAc (50 mL/mmol). The organic layers were combined, dried with $MgSO_4$ and concentrated using rotary evaporation. The crude product was purified by column chromatography.

Procedure E (N-Boc deprotection) The N-Boc protected tetrazine was dissolved in dry DCM (1 mL/30 mg) and a 4M HCl in dioxane solution (1 mL / 30 mg) was added dropwise over 1 minute while stirring at room temperature. The reaction mixture was stirred at room temperature for 2 hours resulting in a suspension. The suspension was centrifuged and the colorless supernatant was removed. The colorful precipitate was washed 2 times via re-suspension in 10 mL of dry dioxane, centrifugation, and partitioning from the colorless supernatant. The precipitate was re-suspended in 5 mL of dry dioxane, transferred to a flask and concentrated using rotary evaporation resulting in quantitative N-Boc deprotected product as an ammonium chloride salt.

General Analytic Procedures

Fluorescence profile Excitation and Emission profiles of AMC **27** and 2-TCO-AMC **28** were determined in DMSO/H_2O and phosphate buffered water at 5 µM concentrations. Excitation wavelength was optimized towards highest ratio (Ex_{25} % / Ex_{24} %). Emission wavelength was optimized to maximize the fluorescence difference Δ % (Em_{25} % – Em_{24} %).

Fluorescence background analysis Background fluorescence of tetrazines was determined in PBS. 5 µl of a 10 mM solution of tetrazine (**4b**-**17b**, **4**-**17**, **1**, **2**, **23**-**25**, **3**, **21**) in DMSO was added

to 195µl PBS. The fluorescence intensity (λ_{ex} = 380 nm, λ_{em} = 450 nm) was determined comparing with **28** (0% elimination) and **27** (100% elimination) in matching solvent.

Elimination efficiency test A The elimination efficiency of tetrazines was determined by incubation of the various tetrazines in the desired solvent (DMSO/H_2O or PBS) at 37 °C over a time period of 8 days. 1.5 µl of a 10 mM solution of 2-TCO-AMC **28** (or AMC **27** as a control) in DMSO was dissolved in 3 mL solvent, followed by 6 µl of a 10 mM solution of tetrazine (**4b**-**17b**, **4**-**17**, **1**, **2**, **23**-**25**; or no tetrazine as a control) in DMSO. The resulting solution was then incubated at 37 °C. At time points 1, 2, 4, 8, 24, 48, 96 and 192 hours 200 µL aliquots were taken and the fluorescence intensity (λ_{ex} = 380 nm, λ_{em} = 450 nm) was determined. The test was performed twice on all tetrazines. Percentage of elimination was determined comparing with **28** (0% elimination) and **27** (100% elimination) in matching solvent.

Elimination efficiency test B The elimination efficiency of tetrazines was determined by incubation in phosphate buffer (0.2M at pH 7.4, 6 or 3) at 25 °C over a time period of 16 hours. 10 µl of a 100 µM solution of 2-TCO-AMC **28** (or AMC **27** as a control) in DMSO was dissolved in 180 µl, followed by addition of 10 µl of a 100 µM solution of tetrazine (**4b**-**7b**, **4**-**7**, **1**, **2**, **23**-**25**, **3**, **21**; or no tetrazine as a control) in DMSO. The fluorescence intensity (λ_{ex} = 380 nm, λ_{em} = 450 nm) was determined over a period of 16 hours at 1 to 5 minute intervals. The test was performed twice on all tetrazines. Percentage of elimination was determined comparing with **28** (0% elimination) and **27** (100% elimination) in matching pH solvent due to pH dependent variable fluorescence of **27**.

Elimination efficiency test C The elimination efficiency of tetrazines was determined by incubation in PBS over a time period of 1 day. 1 µl of of a 10 mM solution of 2-TCO-AMC **28** in DMSO, 10 µl of a 10 mM solution of tetrazine (**1**, **2**, **3**, **5**, **6** or **7**) in DMSO and 99 µl of PBS (pH = 7.4) were incubated in an LCMS vial and measured by C18 column LC-MS analysis using a freshly made 2.5 mM ammonium formate buffer solution (pH = 8.4 titrated using conc. NH_4OH (aq.)) and acetonitrile as eluent components. 5 µl of the solution was injected at t = 5, 30, 60, 240, 960 minutes. Intermediates and products formed were identified by mass analysis and aminomethyl coumarin bearing compounds were quantified by UV analysis.

HRMS analysis of analytically unstable tetrazines Tetrazines that could not be identified by HRMS were reacted with 4-OH-TCO at 1mM concentration to form a non-eliminating adduct for HRMS.

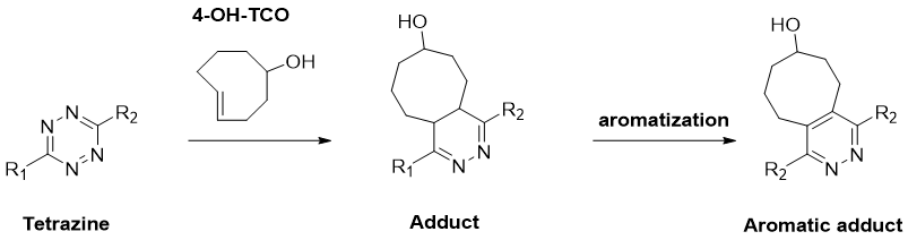

Procedure: For each tetrazine 160 µl DMSO was placed in a small vial and 20 µl of 10mM tetrazine solution was added, followed by 20 µl of 10mM 4-OH-TCO. Near-instantaneous

discoloration was observed, where after the vials were stored at -20 °C until HRMS analysis was performed. Due to aromatizing effects of the product tetrazines were identified by **adduct mass** (m/z) or **aromatic adduct mass** (m/z -2).

Compound Synthesis

Compound 3: Synthesis was performed in a closed pressure tube (**procedure B**) at 60 °C overnight. 1.0 mmol (0.099 g) of compound **22**, 10 mmol (0.26 ml, 0.21 g) of acetonitrile, 0.25 mmol (0.090 g) nickel triflate, 1.5 mL of dioxane and 47 mmol (1.5 mL, 1.5 g) of anhydrous hydrazine were used. Oxidation (**procedure C**) was performed using 40 mL of DCM/AcOH (1:1, v:v) and 22 mmol (1.5 g) of solid $NaNO_2$. Purification was performed with silica column chromatography using an 2:20:78 AcOH:EtOAc:DCM eluent resulting in 0.008 g (0.047 mmol, 4.7%) of compound **3** as a pink solid. ^{1}H NMR (500 MHz, MeOD) δ 3.56 (t, *J* = 7.0 Hz, 2H, CH_2), 3.03 (t, *J* = 7.0 Hz, 2H, CH_2), 2.98 (s, 3H, CH_3). ^{13}C NMR (126 MHz, MeOD) δ 176.03, 170.17, 168.98, 31.64, 30.79, 21.12. HRMS (m/z): adduct $[C_{14}H_{22}N_2O_3 + H]^+$ calculated 267.1703, found 267.1704.

Compound 16b: *For synthesis details, see **Compound 12b**.* ^{1}H NMR (400 MHz, $CDCl_3$) δ 5.68 (s, 2H, NH), 4.95 (d, *J* = 5.6 Hz, 4H, CH_2), 1.43 (s, 18H, Boc, CH_3). ^{13}C NMR (101 MHz, $CDCl_3$) δ 167.71, 155.93, 80.50, 43.57, 28.40. HRMS (m/z): $[C_{14}H_{24}N_6O_4 + Na]^+$ calculated 363.1752, found 363.1759.

Compound 16: N-Boc deprotection of compound **16b** was performed using 4M HCl in dioxane according to **procedure E** obtaining compound **16** in quantitative yield as a bright pink solid. ^{1}H NMR (400 MHz, DMSO) δ 9.16 (s, 6H, NH_3Cl), 4.82 (s,4H, CH_2). ^{13}C NMR (101 MHz, DMSO) δ 165.09, 40.94. HRMS (m/z): $[C_4H_8N_6 + H]^+$ calculated 141.0883, found 141.0880.

Compound 17b: (*Alternative synthesis for **Compound 6b**)* Synthesis was performed in a closed pressure tube (**procedure B**) at 60 °C overnight. 2.02 mmol (0.344 g) of compound **18**, 12 mmol (1.0 ml, 1.1 g) of 2-pyridinecarbonitrile, 0.48 mmol (0.173 g) zinc triflate, 3.0 mL of dioxane and 101 mmol (3.2 mL, 3.2 g) of anhydrous hydrazine were used. Oxidation (**procedure D**) was performed using 80 mmol (20 mL) of 4M $NaNO_2$ (aq.) and 120 mmol (60 mL) 2M HCl (aq.). Purification was performed with silica column chromatography using an 10% to 60% EtOAc/Pentane eluent resulting in 0.034 g (0.11 mmol, 5.4%) of compound **6b** as a pink oil and 0.074 g (0.20 mmol, 19.8%) of compound **17b** as a red solid byproduct. **TLC**: Compound **6b** Rf = 0.2, compound **17b** Rf = 0.5, 50% EtOAc in pentane. ^{1}H NMR (400 MHz, $CDCl_3$) δ 5.12 (s, 2H, NH), 3.71 (dd, *J* = 12.3, 6.2 Hz, 4H, CH_2), 3.49 (t, *J* = 6.1 Hz, 4H, CH_2), 1.35 (s, 18H, Boc, CH_3). ^{13}C NMR (101 MHz, $CDCl_3$) δ 168.48, 155.90, 79.58, 38.50, 35.61, 28.42. HRMS (m/z): $[C_{16}H_{28}N_6O_4 + Na]^+$ calculated 391.2065, found 391.2070.

Compound 17: N-Boc deprotection of compound **17b** was performed using 4M HCl in dioxane according to **procedure E** obtaining compound **17** in quantitative yield as a pink solid. ^{1}H NMR (400 MHz, DMSO) δ 8.31 (s, 6H, NH_3Cl), 3.66 (t, *J* = 6.9 Hz, 4H, CH_2), 3.47 – 3.31 (m, 4H, CH_2). ^{13}C NMR (101 MHz, DMSO) δ 166.89, 37.00, 32.11. HRMS (m/z): $[C_6H_{12}N_6 + H]^+$ calculated 169.1197, found 169.1199.

Compound 21: Synthesis was performed in a closed pressure tube (**procedure B**) at 30 °C for 3 days. 7.87 mmol (0.780 g) of compound **22**, 0.25 mmol (0.086 g) zinc triflate, 1.5 mL of dioxane and 47 mmol (1.5 mL, 1.5 g) of anhydrous hydrazine were used. Oxidation (**procedure C**) was performed using 40 mL of DCM/AcOH (1:1, v:v) and 22 mmol (1.5 g) $NaNO_2$ (s). Purification was performed with silica column chromatography using an AcOH:EtOAc:DCM eluent resulting in 0.210 g (0.928 mmol, 23.6%) of compound **21** as a pink solid. ^{1}H NMR (400 MHz, DMSO) δ 3.47 (t, *J* = 6.8 Hz, 4H, CH_2), 2.90 (t, *J* = 6.8 Hz, 4H, CH_2). ^{13}C NMR (101 MHz, DMSO) δ 173.43, 168.73, 30.56, 29.40. HRMS (m/z): adduct $[C_{16}H_{24}N_2O_5 + H]^+$ calculated 325.1758, found 325.1767.

Compound 22: Following literature procedure[22], 300 mmol (44.14 g) of D-glutamic acid was dissolved in a solution of 300 mL 2M NaOH (aq.) (600 mmol) and portionwise over 30 minutes 200 mmol (48 g) of trichloroisocyanuric acid (TCCA) was added while stirring at room temperature in a water bath. The reaction was very exothermic and heavy foaming occurred. The reaction mixture was stirred for an additional 30 minutes, where after 50 mL of con. HCl (aq.) (600 mmol) was added. The reaction mixture was extracted with EA, dried using $MgSO_4$ and concentrated under rotary evaporation resulting in 22.72 g (229.3 mmol, 76.4%) of compound **22** as a pale yellowish solid. ^{1}H NMR (400 MHz, $CDCl_3$) δ 11.13 (s, 1H, COOH), 2.72 (t, *J* = 6.7 Hz, 2H, CH_2), 2.62 (t, *J* = 6.8 Hz, 2H, CH_2). ^{13}C NMR (101 MHz, $CDCl_3$) δ 175.69, 118.46, 29.56, 12.62.

Compound 23: *For synthesis details, see **Compound 14b**.* ^{1}H NMR (400 MHz, $CDCl_3$) δ 8.93 (d, *J* = 4.2 Hz, 2H, pyr, CH), 8.70 (d, *J* = 7.9 Hz, 2H, pyr, CH), 7.97 (ddd, *J* = 7.8, 7.8, 1.6 Hz, 2H, pyr, CH), 7.54 (ddd, *J* = 7.5, 4.7, 0.7 Hz, 2H, pyr, CH). ^{13}C NMR (101 MHz, $CDCl_3$) δ 163.86, 151.04, 150.03, 137.55, 126.66, 124.55. HRMS (m/z): $[C_{12}H_8N_6 + H]^+$ calculated 237.0884, found 237.0892.

Compound 28: 0.21 mmol (37 mg) of aminomethylcoumarin **27**, 0.71 mmol (75 mg) of solid Na_2CO_3 and 0.14 mmol (42 mg) of triphosgene were dissolved in 4 mL DCM at 0 °C and stirred for 4 hours while warming to room temperature. The reaction mixture was reduced by rotary evaporation and redissolved in 2 mL THF. 0.15 mmol (19 mg) of 2-hydroxy-*trans*cyclooctene (2-OH-TCO, **26**) and 0.60 mmol (84 µl, 61 mg) of TEA were added and the reaction mixture was stirred overnight at room temperature. The reaction mixture was reduced under rotary evaporation, purified with silica column chromatography using an 10% to 40% EtOAc/Pentane eluent resulting in 2.3 mg (7.0 µmol, 4.7%) of compound **28** as a pale solid. ^{1}H NMR (850 MHz, $CDCl_3$) δ 7.53 (d, *J* = 8.6 Hz, 1H), 7.45 (s, 1H), 7.40 (d, *J* = 1.9 Hz, 1H), 6.96 (s, 1H), 6.19 (d, *J* = 0.8 Hz, 1H), 5.91 – 5.86 (m, 1H), 5.58 (dd, *J* = 16.5, 2.2 Hz, 1H), 5.46 (s, 1H), 2.51 – 2.47 (m, 1H), 2.41 (d, *J* = 0.8 Hz, 3H), 2.14 (dd, *J* = 15.0, 4.2 Hz, 1H), 2.08 – 2.02 (m, 1H), 2.02 – 1.98 (m, 1H), 1.93 – 1.87 (m, 1H), 1.80 – 1.74 (m, 1H), 1.73 – 1.68 (m, 1H), 1.54 – 1.47 (m, 1H), 1.14 – 1.09 (m, 1H), 0.86 – 0.81 (m, 1H). ^{13}C NMR (214 MHz, $CDCl_3$) δ 161.27, 154.57, 152.39, 152.29, 141.62, 132.51, 130.70, 125.54, 115.60, 114.42, 113.26, 105.88, 75.15, 40.75, 36.13, 36.08, 29.16, 24.32, 18.76. HRMS (m/z): $[C_{19}H_{21}NO_4 + H]^+$ calculated 328.1543, found 328.1551.

References

[1] a) D.M. Paterson, L.A. Nazarova, J.A. Prescher, *ACS Chem. Biol.* **2014**, 9, 592-605, b) X. Fan, J. Li, P.R. Chen, *Natl. Sci. Rev.* **2017**, 4, 300-302.

[2] a) C. W. Tornøe, C. Christensen, M. Meldal, *J. Org. Chem.*, **2002**, 67, 3057–3064, b) V. V. Rostovtsev, L. G. Green, V. V. Fokin, K. B. Sharpless, *Angew. Chem. Int. Ed.*, **2002**, 41, 2596–2599, c) J.E. Hein, V.V. Fokin, *Chem. Soc. Rev.*, **2010**, 39, 1302-1315.

[3] a) E. Saxon, C. R. Bertozzi, *Science*, **2000**, 287, 2007–2010 b) E. Saxon, C. R. Bertozzi, *Org. Lett.,* **2000**, 2, 2141-2143, c) C.I. Schilling, N. Jung, M. Biskup, U. Schepers, S. Bräse, *Chem. Soc. Rev.*, **2011**, 40, 4840-4871.

[4] a) M.L. Blackman, M. Royzen, J.M. Fox, *J. Am. Chem. Soc.*, **2008**, *130,* 13518-13519, b) N. K. Devaraj, R. Weissleder, S. A. Hilderbrand, Bioconjugate Chem., 2008, 19, 2297–2299, c) S. Mayer, K. Lang, *Synthesis*, **2017**, *49*, 830-848.

[5] a) E.M. Sletten, C.R. Bertozzi, *Acc. Chem. Res.*, **2011**, 44, 666-676, b) K. Lang, J.W. Chin, *ACS Chem. Biol.*, **2014**, 9, 16-20, c) G.B. Cserép, A Herner, P Kele, Methods Appl, Fluoresc., 2015, 3, 042001.

[6] J. Li, P.R. Chen, *Nat. Chem. Bio.*, **2016**, 12, 129-137.

[7] R.M. Versteegen, R. Rossin, W. ten Hoeve, H.M. Janssen, M.S. Robillard, *Angew. Chem. Int. Ed.*, **2013**, 52, 14112-14116.

[8] A.M.F. van der Gracht, M.A.R. de Geus, M.G.M. Camps, T.J. Ruckwardt, A.J.C. Sarris, J. Bremmers, E. Maurits, J.B. Pawlak, M.M. Posthoorn, K.M. Bonger, D.V. Filippov , H.S. Overkleeft, M.S. Robillard, F. Ossendorp, S.I. van Kasteren, *ACS Chem. Biol.*, **2018**, 13, 1569-1576.

[9] L. Liu, Y. Liu, G. Zhang, Y. Ge, X. Fan, F. Lin, J. Wang, H. Zheng, X. Xie, X. Zeng, P.R. Chen, *Biochemistry*, **2018**, 57, 446-450.

[10] G. Zhang, J. Lie, R. Xie, X. Fan, Y. Liu, S. Zheng, Y. Ge, P.R. Chen, *ACS Cent. Sci.*, **2016**, 2, 325-331.

[11] a) R. Rossin, S.M.J. van Duijnhoven, W. ten Hoeve, H.M. Janssen, L.H.J. Kleijn, F.J.M. Hoeben, R.M. Versteegen, M.S. Robillard, *Bioconjugate Chem.*, **2016**, 27, 1697-1706, b) I. Khan, L.M. Seebald, N.M. Robertson, M.V. Yigit, M. Royzen, *Chem. Sci.*, **2017**, 8, 5705-5712, c) R. Rossin, R.M. Versteegen, J. Wu, A. Khasanov, H.J. Wessels, E.J. Steenbergen, W. ten Hoeve, H.M. Janssen, A.H.A.M. van Onzen, P.J. Hudson, M.S. Robillard, *Nat. Commun.*, **2018**, 9, 1484.

[12] J.M. Mejia Oneto, I. Khan, L. Seebald, M. Royzen, *ACS Cent. Sci.*, **2016**, 2, 476-482.

[13] a) X. Fan, Y. Ge, F. Lin, Y. Yang, G. Zhang, W.S.C. Ngai, Z. Lin, S. Zheng, J. Wang, J. Zhao, J. Lie, P.R. Chen, *Angew. Chem. Intl. Ed.*, **2016**, 55, 14046-14050, b) J.C.T. Carlson, H. Mikula, R. Weissleder, *J. Am. Chem. Soc.*, **2018**, 140, 3603-3612, c) R.M. Versteegen, W. ten Hoeve, R. Rossin, M.A.R. de Geus, H.M. Janssen, M.S. Robillard, *Angew. Chem. Intl. Ed.*, **2018**, 57, 1.

[14] a) M.T. Taylor, M.L. Blackman, O. Dmitrenko, J.M. Fox, *J. Am. Chem. Soc.*, **2011**, 133, 9646; b) F. Liu, Y. Liang, K.N. Houk, *J. Am. Chem. Soc.*, **2014**, 136, 11483.

[15] R.E. Bird, S.A. Lemmel, X. Yu, Q. A. Zhou, *Bioconjugate Chem.*, **2021**, 32, 2457−2479.

[16] A.M.F. van der Gracht, M.A.R. de Geus, M.G.M. Camps, T.J. Ruckwardt, A.J.C. Sarris, J. Bremmers, E. Maurits, J.B. Pawlak, M.M. Posthoorn, K.M. Bonger, D.V. Filippov, H.S. Overkleeft, M.S. Robillard, F. Ossendorp, S.I. van Kasteren, *ACS Chem. Biol.*, **2018**, 13, 1569.

[17] Spartan '10, J. Kong et. al., Wavefunction Inc., **2004**.

[18] Gaussian 09, M. J. Frisch, G. W. Trucks, H. B. Schlegel, G. E. Scuseria, M. A. Robb, J. R. Cheeseman, G. Scalmani, V. Barone, G. A. Petersson, H. Nakatsuji, X. Li, M. Caricato, A. Marenich, J. Bloino, B. G. Janesko, R. Gomperts, B. Mennucci, H. P. Hratchian, J. V. Ortiz, A. F. Izmaylov, J. L. Sonnenberg, D. Williams-Young, F. Ding, F. Lipparini, F. Egidi, J. Goings, B. Peng, A. Petrone, T. Henderson, D. Ranasinghe, V. G. Zakrzewski, J. Gao, N. Rega, G. Zheng, W. Liang, M. Hada, M. Ehara, K. Toyota, R. Fukuda, J. Hasegawa, M. Ishida, T. Nakajima, Y. Honda, O. Kitao, H. Nakai, T. Vreven, K. Throssell, J. A.

Montgomery, Jr., J. E. Peralta, F. Ogliaro, M. Bearpark, J. J. Heyd, E. Brothers, K. N. Kudin, V. N. Staroverov, T. Keith, R. Kobayashi, J. Normand, K. Raghavachari, A. Rendell, J. C. Burant, S. S. Iyengar, J. Tomasi, M. Cossi, J. M. Millam, M. Klene, C. Adamo, R. Cammi, J. W. Ochterski, R. L. Martin, K. Morokuma, O. Farkas, J. B. Foresman, and D. J. Fox, Gaussian, Inc., Wallingford CT, **2016**.

[19] S. Grimme, *J. Computational Chem.*, **2006**, 27, 1787.

[20] CYLview, 1.0b; C.Y. Legault, Université de Sherbrooke, **2009**. (http://www.cylview.org)

[21] a) M.T. Taylor, M.L. Blackman, O. Dmitrenko, J.M. Fox, *J. Am. Chem. Soc.*, **2011**, 133, 9646; b) F. Liu, Y. Liang, K.N. Houk, *J. Am. Chem. Soc.*, **2014**, 136, 11483.

[22] L. De Luca, G. Giacomelli, *Synlett*, **2004**, 12, 2180.